Applied Mathematics and Computation 268 (2015) 1267–1281

Contents lists available at ScienceDirect

Applied Mathematics and Computation

journal homepage: www.elsevier.com/locate/amc

Parameter identification of BIPT system using chaotic-enhanced fruit fly optimization algorithm☆

Xiaofang Yuan[a,*], Yuanming Liu[a], Yongzhong Xiang[a], Xinggang Yan[b]

[a] College of Electrical and Information Engineering, Hunan University, Changsha 410082, China
[b] School of Engineering and Digital Arts, University of Kent, Kent, United Kingdom

ARTICLE INFO

Keywords:
Parameter identification
Fruit fly optimization algorithm (FOA)
Bidirectional inductive power transfer (BIPT)
Multi-dimensional optimization
Chaotic sequence

ABSTRACT

Bidirectional inductive power transfer (BIPT) system facilitates contactless power transfer between two sides and across an air-gap, through weak magnetic coupling. Typically, this system is nonlinear high order system which includes nonlinear switch components and resonant networks, developing of accurate model is a challenging task. In this paper, a novel technique for parameter identification of a BIPT system is presented by using chaotic-enhanced fruit fly optimization algorithm (CFOA). The fruit fly optimization algorithm (FOA) is a new meta-heuristic technique based on the swarm behavior of the fruit fly. This paper proposes a novel CFOA, which employs chaotic sequence to enhance the global optimization capacity of original FOA. The parameter identification of the BIPT system is formalized as a multi-dimensional optimization problem, and an objective function is established minimizing the errors between the estimated and measured values. All the 11 parameters of this system (L_{pi}, L_T, L_{si}, L_{so}, C_T, C_s, M, R_{pi}, R_T, R_{si} and R_{so}) can be identified simultaneously using measured input–output data. Simulations show that the proposed parameter identification technique is robust to measurements noise and variation of operation condition and thus it is suitable for practical application.

1. Introduction

Inductive power transfer (IPT) is a kind of new technology that has obtained global acceptance and popularity as a technique, which is suitable for supplying power to variety of applications without physical contacts [1,2]. This technology transfers power from one system to another across an air-gap through weak magnetic coupling. IPT system has the potential advantages of high efficiency, high reliability and robustness even when it is in hostile environments [3]. In the past years, many uni-directional IPT systems, with various circuit topologies or compensation strategies and levels of sophistication in control, have been developed in different applications, which range from very low power bio-medical implants to high power battery charging system [1–3]. Recently, bidirectional IPT (BIPT) system has also been proposed and implemented for applications such as V2G system [4,5]. Generally, power handling capability of BIPT system is improved through either series or parallel compensations and, therefore, this kind of system usually operates as high order resonant circuit and at high frequency. Consequently, BIPT system is complex and difficult to design. For the effective analysis of BIPT system, accurate parameter model is essentially required. As the BIPT

☆ This work was supported in part by the National Natural Science Foundation of China (No. 61104088).
* Corresponding author. Tel.: +86 13873195923.
E-mail address: yuanxiaofang126@126.com, yuanxiaofang@hnu.edu.cn (X. Yuan).

http://dx.doi.org/10.1016/j.amc.2015.07.030
0096-3003/

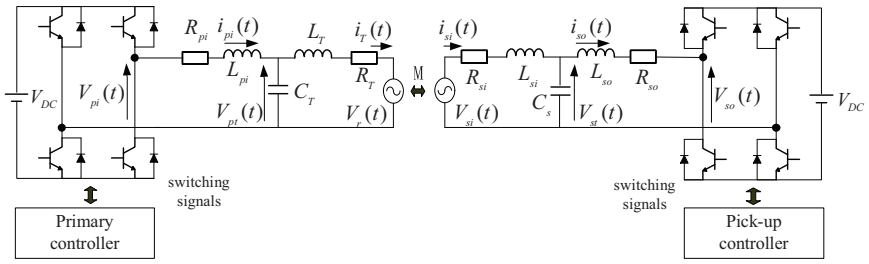

Fig. 1. A typical BIPT system.

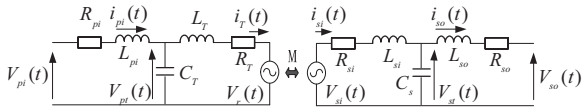

Fig. 2. Equivalent circuit representation of BIPT system.

system also is nonlinear high order system which includes nonlinear switch components and resonant networks, developing of accurate model of this system is a challenging task.

In the last few decades, more and more researches suggest that nature is a great source for inspirations to meta-heuristic techniques [6]. Biologically-inspired meta-heuristic techniques are covering terms for different computational methods that are based on principles or models of biological systems, some examples include but not limited to ant colony optimization (ACO) [7,8], artificial bee colony algorithm (ABC) [9,10], genetic algorithm (GA) [11,12], Firefly algorithm (FA) [13], bacterial gene recombination algorithm (BGRA) [14], bumble bees mating optimization (BBMO) algorithm [15], social spider algorithm [16] etc. More recently, a new kind of Drosophila (fruit fly) inspired swarm intelligence technique has been developed, called fruit fly optimization algorithm (FOA) [17]. The main inspiration of FOA is that the fruit fly itself is superior to other species in sensing and perception, especially in osphresis and vision [18,19]. Since FOA is simple and elegant in concept, easy to implement and has few parameters, it has been applied in many areas [20–24]. In order to improve the exploration and exploitation ability, several kinds of improved FOA were proposed in [24–27]. However, FOA or improved FOA usually performs local optimum or premature in solving multi-dimensional optimization problem. Considering this weakness of FOA, in this paper, a novel chaotic-enhanced fruit fly optimization algorithm (CFOA) is proposed, which uses ergodic property of chaotic sequences to enhance the global optimization capacity of original FOA.

In this paper, the parameter identification problem is formalized as a multi-dimensional optimization problem, which is solved using the proposed CFOA technique. For the parameter identification of the BIPT system, an objective function is established minimizing the errors between the estimated and measured values. All the 11 parameters of this system (L_{pi}, L_T, L_{si}, L_{so}, C_T, C_s, M, R_{pi}, R_T, R_{si} and R_{so}) can be identified simultaneously using measured input–output data. The proposed CFOA is used to search the optimal parameters values of this system using measured input–output data. The implementation of the CFOA based parameter identification technique is analyzed in detail, and different chaotic sequences for CFOA have also been tested in the simulation.

The remaining of this paper is organized as follows. Model of a typical BIPT system is described in Section 2. Review of original FOA is summarized in Section 3. Section 4 describes the motivation and implementation of the CFOA technique. In Section 5, CFOA based parameter identification of BIPT system is described. The testing of the proposed parameter identification technique is carried out and the simulation results are shown in Section 6. Finally, Section 7 concludes the paper.

2. Model of typical BIPT system

The schematic of a BIPT system presented in [4] is shown in Fig. 1. The output of the pick-up circuit is connected to the load, which is denoted as a DC supply to either deliver or absorb power. Analogous to a BIPT system, a primary supply generates a constant track current $i_T(t)$ in L_T, which is magnetically coupled with the pick-up coil. The primary and pick-up circuits are implemented with virtually identical electronics, which include a reversible rectifier and a tuned inductor–capacitor–inductor (LCL) circuit, to facilitate bidirectional power flow between the track and the pick-up. The primary and pick-up system can thus be represented by the circuit model in [5] illustrated in Fig. 2.

The dynamic model of this system is developed by introducing the state variables as [3]:

$$\begin{aligned} x &= [x_1\ x_2\ x_3\ x_4\ x_5\ x_6\ ]^T \\ &= [i_{pi}\ i_T\ V_{pt}\ i_{si}\ i_{so}\ V_{st}] \end{aligned} \tag{1}$$

where $x_1 = i_{pi}$ is the current through the primary side inductor L_{pi}, $x_2 = i_T$ is the current through track inductor L_T, $x_3 = V_{pt}$ is the voltage across the primary side capacitor C_T, $x_4 = i_{si}$ is the current through the secondary side inductor L_{si}, $x_5 = i_{so}$ is the current through the pick-up side inductor L_{so}, $x_6 = V_{st}$ is the voltage across the pick-up side capacitor C_s.

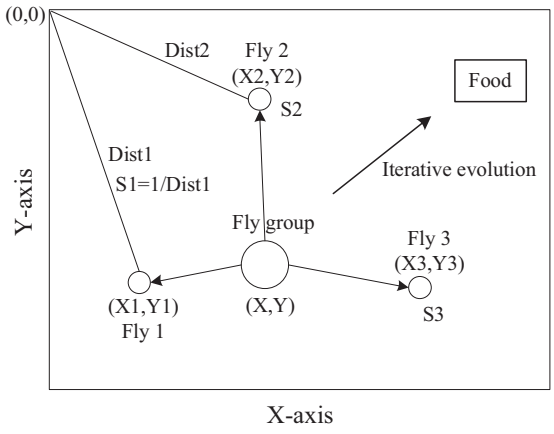

Fig. 3. The group iterative food searching of fruit flies.

Let the input vector u be $u = [u_1\ u_2]^T$ as:

$$u = [u_1\ u_2]^T = [V_{pi}\ V_{so}]^T \tag{2}$$

where $u_1 = V_{pi}$ is the input voltage applied at the primary side. Note that this voltage is essentially the output voltage of the primary side converter and $u_2 = V_{so}$ is the voltage at the pick-up side. Consider the track current $x_2 = i_T$ and pickup current $x_5 = i_{so}$ as outputs. The output equation can be given by:

$$y = [y_1\ y_2]^T = [i_T\ i_{so}]^T \tag{3}$$

Following the basic principle of circuit theory, the dynamic model of this system is expressed by the following eighth order differential equations [3]:

$$\begin{aligned}
\dot{x}_1 &= -\frac{R_{pi}}{L_{pi}}x_1 - \frac{1}{L_{pi}}x_3 + \frac{1}{L_{pi}}u_1 \\
\dot{x}_2 &= \gamma\left[-\frac{R_T}{L_T}x_2 + \frac{1}{L_T}x_3 - \beta R_{si}x_4 - \beta x_6\right] \\
\dot{x}_3 &= \frac{1}{C_T}x_1 - \frac{1}{C_T}x_2 \\
\dot{x}_4 &= \gamma\left[-\beta R_T x_2 + \beta x_3 - \frac{R_{si}}{L_{si}}x_4 - \frac{1}{L_{si}}x_6\right] \\
\dot{x}_5 &= -\frac{R_{so}}{L_{so}}x_5 + \frac{1}{L_{so}}x_6 - \frac{1}{L_{so}}u_2 \\
\dot{x}_6 &= \frac{1}{C_s}x_4 - \frac{1}{C_s}x_5
\end{aligned} \tag{4}$$

where $\beta = \frac{M}{L_{si}L_T}$, $\gamma = \frac{1}{1-M\beta}$, and M represents the magnetic coupling between the track inductance and pick-up coil inductance. The parameter vector appears nonlinearly in these equations, and it can be seen from Eq. (4) that in this system, there are totally 11 variables which need to be identified: L_{pi}, L_T, L_{si}, L_{so}, C_T, C_s, M, R_{pi}, R_T, R_{si} and R_{so}.

3. Original FOA technique

The FOA is a new population based heuristic algorithm discovered through simulation of the intelligent foraging behavior of fruit fly. The group iterative food searching of fruit flies in two-dimension according to FOA has been graphically shown in Fig. 3.

Based upon the Drosophila's biological behavior, the main motivation of FOA technique is as follows [17]: (1) The fly flies with *Lévy* flight motion; (2) it smells the potential location (attractiveness); (3) it would then taste. If it is not to its liking (fitness/profitability), it rejects and goes to another location. To the fly, attractiveness is not necessarily profitable; (4) while foraging or mating, the fly also sends and receives messages with its friends about its food and their mates. The original FOA in [17,20–23] can be divided into several necessary steps and the main steps are described as follows:

Step 1. Random initial fruit fly swarm location. *Init X_axis*; *Init Y_axis*.

Step 2. Give the random direction and distance for the search of food using osphresis by an individual fruit fly

$$X_i = X\_axis + RandomValue \tag{5}$$

$$Y_i = Y\_axis + RandomValue \tag{6}$$

where i is the population size of fruit flies.

Step 3. Since the food location cannot be known, the distance to the origin is thus estimated first ($Dist_i$), then the smell concentration judgment value (S_i) is calculated, and this value is the reciprocal of distance

$$Dist_i = \sqrt{X_i^2 + Y_i^2} \tag{7}$$

$$S_i = \frac{1}{Dist_i} \tag{8}$$

Step 4. Substitute smell concentration judgment value (S_i) into smell concentration judgment function (or called objective function) in order to find the smell concentration ($Smell_i$) of the individual location of the fruit fly.

$$Smell_i = Function(S_i) \tag{9}$$

Step 5. Find out the fruit fly with maximal smell concentration(finding the maximal value) among the fruit fly swarm.

$$[bestSmell\ bestIndex] = max(Smell) \tag{10}$$

Step 6. Keep the best smell concentration value and x, y coordinate,and at this moment, the fruit fly swarm will use vision to fly toward that location.

$$Smellbest = bestSmell \tag{11}$$

$$X\_axis = X(bestIndex) \tag{12}$$

$$Y\_axis = Y(bestIndex) \tag{13}$$

Step 7. Enter iterative optimization to repeat the implementation of **Steps 2**–**5**, then judge whether the smell concentration is superior to the previous iterative smell concentration. If yes, go to **Step 6**.

4. Proposed CFOA technique

4.1. Chaotic sequence

The ergodicity of chaos implies that chaotic sequence can traverse all the state of strange attractor and search a whole range of design space. This basic property is utilized to search for a global optimum in chaos optimization algorithm [28,29]. Mathematically, chaos is randomness of a simple deterministic dynamical system and chaotic sequence may be considered as sources of randomness [30]. One-dimensional chaotic sequence is the simplest system with the capability of generating chaotic motion. In this study, the following six kinds of different chaotic sequences are used [31]:

(1) Logistic sequence:

$$x_{n+1} = 4x_n(1 - x_n),\ x_n \in (0, 1) \tag{14}$$

(2) Tent sequence:

$$x_{n+1} = x_n/0.7,\ x_n < 0.7$$
$$x_{n+1} = \left(\frac{10}{3}\right)x_n(1 - x_n),\ x_n \geq 0.7 \tag{15}$$

(3) Chebyshev sequence:

$$x_{n+1} = \cos\left(5\cos^{-1}x_n\right),\ x_n \in [-1, 1] \tag{16}$$

(4) Cubic sequence:

$$x_{n+1} = 2.59x_n\left(1 - x_n^2\right),\ x_n \in (0, 1) \tag{17}$$

(5) ICMIC sequence:

$$x_{n+1} = \sin\left(\frac{70}{x_n}\right),\ x_n \in (-1, 1) \tag{18}$$

(6) Sinusodial sequence:

$$x_{n+1} = \sin(\pi x_n),\ x_n \in (0, 1) \tag{19}$$

4.2. Motivations

Based on simulations and analysis, the original FOA usually performs local optimum or premature in solving multi-model problem [25]. In this paper, a novel CFOA is proposed, which uses ergodic property of chaos to enhance global optimization capacity of FOA. In this section, several improvements to FOA using chaos theory are pointed out as follows:

4.2.1. Chaos based population initialization

Population initialization is a crucial task in evolutionary algorithm because it may affect the convergence speed and the quality of the final solution. If no any information about the solutions is available, then random initialization is the most commonly used way. To ensure good starting points, the flies in CFOA are distributed and dispatched based on chaotic sequence as:

$$X\_axis_i = L_i + M(\cdot)(U_i - L_i) \tag{20}$$

$$Y\_axis_i = L_i + M(\cdot)(U_i - L_i) \tag{21}$$

where U_i and L_i are the upper and lower limits of variables, and $M(\cdot)$ is the chaotic sequence in Eqs. (14)–(19). Benefiting from the properties of ergodicity and pseudo-randomness, chaotic sequence based initialization can increase the population diversity.

4.2.2. Chaos search technique based exploring

In the FOA, the foraging behavior of fruit flies pulls many flies to swarm together toward the previous best region (X_axis_i, Y_axis_i) as in Step 2. Then, the swarm converges to that position. This aggregation effect brings a fast FOA convergence speed. However, it results in local optimum or premature for multi-model problem. In other words, the previous best position (X_axis, Y_axis) may guide fruit flies into the local minima. To emphasize this concerning issue, chaos search technique is applied to improve the exploration and to jump out of the local minima quickly. In this study, chaos based random direction and distance for the flies swarm using osphresis is given by:

$$X_i = X\_axis_i + M(\cdot) \cdot R(k) \tag{22}$$

$$Y_i = Y\_axis_i + M(\cdot) \cdot R(k) \tag{23}$$

where $R(k)$ is exploring radius using osphresis. The previous best position X_axis_i, Y_axis_i is used as the starting point to execute the chaos search technique based exploring, which can easily promote exploration ability.

4.2.3. Mutative-scale of exploring radius

In this paper, multi-scale exploring radius $R(k)$, that is:

$$R(k) = \frac{U_i - L_i}{2} * \left(\frac{k_{\max} - k}{k_{\max}}\right)^{\phi} \tag{24}$$

where ϕ take value between 2 and 6. A suitable $R(k)$ usually provides a balance between exploration and exploitation. Here $R(k)$ is set as a multi-scale factor according to the iterations number k. It will decrease with the increase of iterations number k. In early iteration, bigger $R(k)$ can increase the diversity of solutions for global exploration, while smaller $R(k)$ in final iteration can increase the fine-tuning of solutions by exploitation.

4.2.4. Modified distance $\mathrm{Dist_i}$ *and smell concentration judgment value* ($\mathrm{S_i}$)

In fact, on the basis of analysis and computations of $Dist_i$ and s_i in Eqs. (7) and (8), it is obvious that numerical values of $Dist_i$ are distributed randomly in large-scale scope. However, the large scope of $Dist_i$ by using $S_i = 1/Dist_i$ in Eq. (8), causing that the scope of S_i becomes very small. When S_i is substituted into fitness function in Eq. (9), this may cause the possibility of the premature or local optimal [23]. In this paper, modified $Dist_i$ and S_i are given by:

$$Dist_i = X_i^2 - Y_i^2 \tag{25}$$

$$S_i = Dist_i \tag{26}$$

Using the modified Eqs. (25) and (26), it is useful for real practical application since decision variable has a large scale searching space. The S_i has the same value of $Dist_i$ with a large scale search space.

4.3. Implementation of CFOA

The implementation procedure of the CFOA is illustrated in Fig. 4. It is summarized as follows (Minimization of objective function is the pursuit).

Step 1. Initialization. Set the max iterations number $k_{\max}$, let $k = 1$. Initialize fruit fly swarm location based on chaotic sequence $M(\cdot)$ as:

$$X\_axis_i = L_i + M(\cdot)(U_i - L_i) \tag{27}$$

$$Y\_axis_i = L_i + M(\cdot)(U_i - L_i) \tag{28}$$

Step 2. Give the random direction and distance for the search of food using osphresis by an individual fruit fly as:

$$X_i = X\_axis_i + R(k) * M(\cdot) \tag{29}$$

$$Y_i = Y\_axis_i + R(k) * M(\cdot) \tag{30}$$

with $R(k) = \frac{U_i - L_i}{2} * (\frac{k_{\max} - k}{k_{\max}})^{\phi}$.

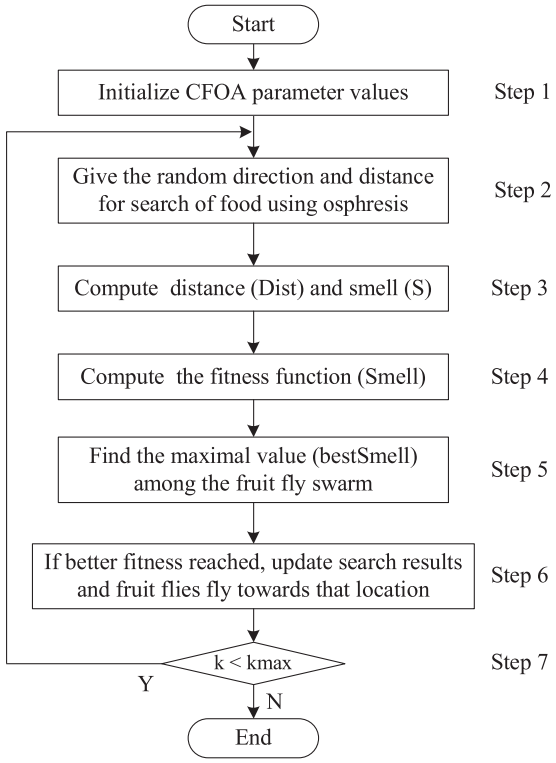

Fig. 4. The implement procedure of the proposed CFOA.

Step 3. The distance $Dist_i$ is then estimated, and the fitness judgment value S_i is calculated by:

$$Dist_i = X_i^2 - Y_i^2 \tag{31}$$

$$S_i = Dist_i \tag{32}$$

Step 4. Substitute fitness judgment value (S_i) into fitness function so as to find the fitness function value ($Smell_i$) of the individual location of the fruit fly.

$$Smell_i = Function(S_i) \tag{33}$$

Step 5. Find out the fruit fly with the minimum value or the best fitness value among the fruit fly swarm.

$$[bestSmell\ bestIndex] = min(Smell) \tag{34}$$

Step 6. Judge if the fitness is superior to the previous iterative fitness, if so, update the best fitness value and at this moment, the fruit fly swarm will use vision to fly towards that location.

$$Smellbest = bestSmell \tag{35}$$

$$X\_axis = X(bestIndex) \tag{36}$$

$$Y\_axis = Y(bestIndex) \tag{37}$$

Step 7. If $k \geq k_{max}$, stop the CFOA search; otherwise, go to **Step 2**.

5. CFOA based parameter identification of a BIPT system

5.1. Parameter identification problem

The dynamic equation of a system for which the parameter value to be identified is assumed to be in the following form:

$$\dot{x} = f(p, x, u)$$
$$y = g(p, x) \tag{33}$$

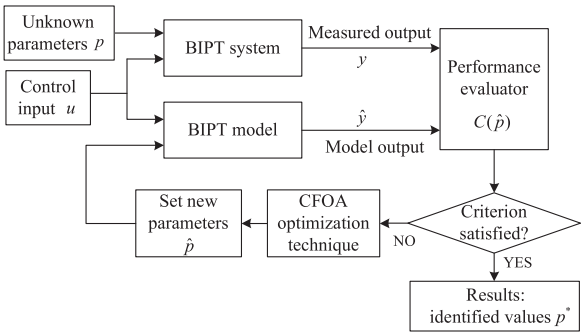

Fig. 5. General identification procedure using CFOA technique.

where u is control input vector, y is system output vector, x is state vector, and p is a column vector containing the parameters to be identified. The system is assumed to be nonlinear, and the parameters may also appear nonlinearly in Eq. (33). To identify parameter vector p, an estimated model of this system is usually introduced as follows:

$$\begin{aligned} \dot{\hat{x}} &= f(\hat{p}, \hat{x}, u) \\ \hat{y} &= g(\hat{p}, \hat{x}) \end{aligned} \tag{34}$$

where $\hat{x}$, $\hat{y}$, and $\hat{p}$ are the estimated values for vector x, y, and p, respectively.

According to Eq. (34), the same control input u is fed into the system model, and the model has the same structure as in Eq. (33), i.e. the same functions $f(.)$ and $g(.)$. The identified parameter vector for unknown p is denoted by $\hat{p}$. For a system with known model structure but unknown parameter value, a popular method for parameter identification is to formulate the problem as an optimization process [32]. Commonly, system output vector y can be measured, and model parameter vector $\hat{p}$ is iteratively varied until the model output $\hat{y}$ well matches the measured output y. The discrepancy between the measured system output y and the estimated model output $\hat{y}$ is minimized with an objective function.

To identify the parameter vector, the following objective function is proposed by minimizing the integral of the absolute difference between the measured system output and estimated system output as:

$$\text{minimize } C(\hat{p}) = \int_0^T (y(t) - \hat{y}(t))^2 dt \tag{35}$$

The goal is to identify the parameter values in the mathematical model such that the outputs of the model closely match the measured data. The identification error will result in a nonzero $C(\hat{p})$, which is used to guide the search for better model parameter $\hat{p}$. Now, it is straight-forward to see that the parameter identification problem for system in Eq. (33) has been transformed into an optimization problem.

5.2. Identification procedure for the BIPT system

The objective now is to discuss how the CFOA technique can be applied to the parameter identification of the BIPT system. From a pure mathematical point-of-view, parameter identification can be formalized as a multi-dimensional optimization problem, typically over real bounded domains. From Eqs. (1)–(4), it follows that a BIPT system usually has known model structure but unknown parameter values. In this paper, the parameter identification of this system is described as a multi-dimensional optimization problem which makes the difference minimum between the model outputs and the measured outputs as shown in Fig. 5.

The parameter identification of the BIPT system is formulated as a multi-dimensional optimization problem given by:

$$\begin{aligned} &\text{minimize} \quad C(\hat{p}) = \sum_{j=1}^{N_s} (y_1(j) - \hat{y}_1(j))^2 + (y_2(j) - \hat{y}_2(j))^2 \\ &\text{subjected to} \qquad L_n \le p_n \le U_n, \quad n = 1, 2, \ldots, 11 \end{aligned} \tag{36}$$

where N_s is the number of sample data, $p = \{L_{pi}, L_T, L_{si}, L_{so}, C_T, C_s, M, R_{pi}, R_T, R_{si}, R_{so}\}$, L_n and U_n are lower and upper limits of variable p_n.

The procedure of the proposed parameter identification technique for the BIPT system is illustrated in Fig. 5. First, the sequent control input u with the number of N_s, is fed into both the actual system and the identified system model. Then, the sequent measured output y and the sequent calculated output $\hat{y}$ with the same number of N_s are input to the performance evaluator, where the fitness function $C(\hat{p})$ will be calculated. If calculated fitness $C(\hat{p})$ is poor, the parameter vector $\hat{p}$ is renewed using CFOA technique and sent to the identified model again. This iterative procedure for improving the parameter vector $\hat{p}$ is stopped if the fitness $C(\hat{p})$ is good enough or it has reached the maximum iterations number of CFOA.

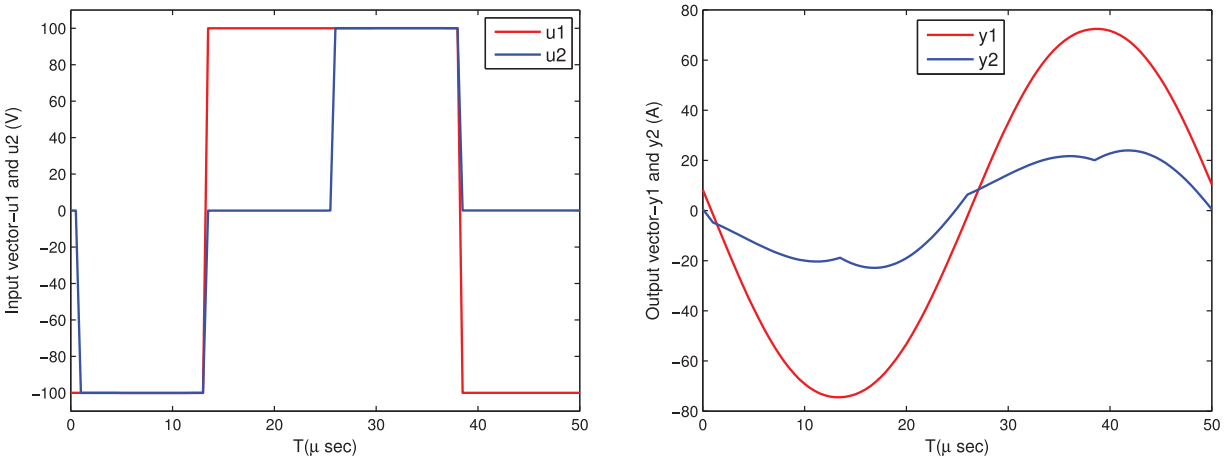

(a) Input vectors u_1 and u_2 (b) Output vectors y_1 and y_2

Fig. 6. Sample dataset for CFOA based parameter identification procedure.

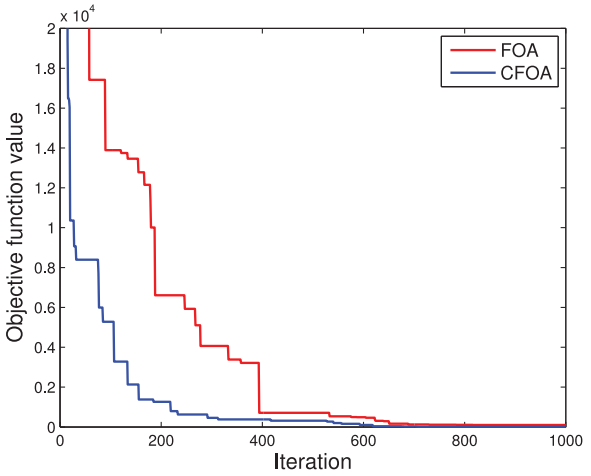

Fig. 7. Typical optimization process of parameter identification using CFOA and FOA.

6. Simulation

In this section, simulations are conducted to evaluate the performance of the proposed parameter identification technique of BIPT system. Prototype parameters of the BIPT system as follows: $L_{pi} = 14.01\ \mu H$, $L_T = 13.7\ \mu H$, $L_{si} = 27.3\ \mu H$, $L_{so} = 27.1\ \mu H$, $C_T = 4.7\ \mu F$, $C_s = 2.43\ \mu F$, $M = 8\ \mu H$, $R_{pi} = 0.0152\ \Omega$, $R_T = 0.0158\ \Omega$, $R_{si} = 0.0179\ \Omega$, $R_{so} = 0.0122\ \Omega$, frequency $= 20$ kHz, $V_{DC,1} = 100$ V, $V_{DC,2} = 100$ V.

Before the parameter identification, there are several important things which need to be considered.

(1) Sample dataset is necessary for CFOA based parameter identification procedure. Periodic control input vectors u_1 and u_2 with the number of 100 are considered in the sample data. In the same time, totally 100 corresponding output vectors y_1 and y_2 of this system are collected as the measured outputs. The input and output vectors of the sample dataset are illustrated in Fig. 6, where sample period $T_{sample} = 0.5\ \mu s$. In Fig. 6, various operation points of this system are included in order to reflect the true state of the system.

(2) Choose the lower and upper limits for variables p to be identified. Choose lower and upper limits of parameters L_{pi}, L_T, L_{si}, L_{so} as 0 and 50 μH, respectively; choose lower and upper limits of parameters C_T and C_s as 0 and 10 μF, respectively; choose lower and upper limits of parameter M as 0 and 20 μH, respectively; choose lower and upper limits of parameters R_{pi}, R_T, R_{si}, R_{so} as 0 and 0.1Ω, respectively.

(3) The CFOA technique is used to search the optimal parameter values to minimize the objective function $C(\hat{p})$ in Eq. (36). The adjustable parameters of the CFOA, obtained by trial, are as follows: $k_{max} = 1000$, population size $i = 100$, $\phi = 4$.

The typical optimization process of parameter identification technique using CFOA is illustrated in Fig. 7, where the FOA based optimization process is also shown for comparison purpose.

Table 1
Comparison among actual p and optimal identified values p^* by CFOA technique.

Item	L_{pi}	L_T	L_{si}	L_{so}	C_T	C_s	M	R_{pi}	R_T	R_{si}	R_{so}
Unit	μH	μH	μH	μH	μF	μF	μH	Ω	Ω	Ω	Ω
Actual p	14.01	13.7	27.3	27.1	4.7	2.43	8.0	0.0152	0.0158	0.0179	0.0122
Identified p^*	13.66	13.73	27.80	27.52	4.72	2.40	7.96	0.0161	0.0149	0.0187	0.0129
IAE	0.35	0.03	0.50	0.42	0.02	0.03	0.04	0.0009	0.0009	0.0008	0.0007
RE (%)	2.50	0.22	1.83	1.55	0.43	1.23	0.50	5.92	5.69	4.47	5.73

Table 2
Parameter identification simulation results using different chaotic sequences for CFOA technique.

Chaotic	RE (%)											Fitness
sequence	L_{pi}	L_T	L_{si}	L_{so}	C_T	C_s	M	R_{pi}	R_T	R_{si}	R_{so}	$C(\hat{p})$
Logistic	2.11	1.93	1.77	2.61	1.82	1.95	2.22	5.12	5.49	5.36	5.27	**16.21**
Tent	2.08	2.24	1.95	1.75	2.18	1.86	2.03	4.79	5.38	4.69	5.62	**15.92**
Chebyshev	1.62	2.04	2.07	1.98	2.25	1.92	2.12	5.28	4.84	4.73	5.80	**16.47**
Cubic	1.84	1.38	1.69	1.92	2.04	2.53	2.30	5.33	6.05	5.87	5.97	**15.88**
ICMIC	1.77	1.93	2.15	1.88	2.23	1.81	2.27	5.64	5.38	4.94	5.25	**16.25**
Sinusodial	1.86	2.17	1.96	1.90	2.28	1.87	2.09	5.14	4.85	5.53	5.74	**16.13**

Table 3
Parameter identification simulation results using different optimization techniques.

Optimization	RE (%)											Fitness
technique	L_{pi}	L_T	L_{si}	L_{so}	C_T	C_s	M	R_{pi}	R_T	R_{si}	R_{so}	$C(\hat{p})$
FOA	3.51	3.67	3.26	3.85	3.94	4.81	3.29	9.12	10.46	8.57	8.62	**36.65**
CFOA	1.84	1.38	1.69	1.92	2.04	2.53	2.30	5.33	6.05	5.87	5.97	**15.88**
ACO	2.57	2.69	2.48	2.75	3.19	3.26	3.43	6.62	6.73	7.30	6.89	**26.37**
ABC	2.59	2.64	2.05	2.60	2.45	3.17	3.26	5.93	6.43	6.28	6.62	**24.69**
GA	2.38	2.55	2.16	2.14	1.89	3.03	2.74	5.48	6.54	5.82	6.11	**22.36**
FA	2.27	2.53	2.68	2.75	2.61	2.96	3.17	5.70	6.25	6.33	6.18	**25.76**
PSO	1.99	2.05	1.98	2.40	2.36	2.74	2.62	5.53	5.84	6.27	5.94	**18.40**

6.1. Case 1: Performance analysis of parameter identification

Two indexes are used to show the parameter identification performance as: individual absolute error IAE $= |x_{\text{actual}} - x_{\text{identified}}|$, relative error RE(%) $= |\frac{x_{\text{actual}} - x_{\text{identified}}}{x_{\text{actual}}}| \times 100\%$.

After the optimization procedure, the optimal identified values p^* by CFOA technique using Tent chaotic sequence have been reported in Table 1, where comparison among actual p and optimal identified values p^* of this system has been reported. Meanwhile, IAE and RE for each variable have also been presented. It can be seen from Table 1 that the unknown parameter values are correctly identified by the proposed CFOA technique. Both IAE and RE are very small, which means that the difference between the actual values and identified ones is very small.

Now, we will compare the simulation results of CFOA technique using six kinds of different chaotic sequences as in Eqs. (14)–(19). All these simulations results have the same iterations number $k_{\max} = 1000$ and population size $i = 100$. Due to stochastic nature, optimization techniques may arrive at better or worse solutions than previously reached solutions during their search for new solutions. For this reason, it is beneficial to run these techniques for many times. The average results of CFOA technique using different chaotic sequences for 20 runs are reported in Table 2, which shows the RE of each variable and fitness value $C(\hat{p})$ as defined in Eq. (36). The results in Table 2 have also verified that CFOA technique using different chaotic sequences can reach good result, therefore, different chaotic sequences can be applied in the CFOA technique.

In addition, we will compare the simulation results of CFOA with other optimization techniques: original FOA, ACO [7], ABC [10], GA [11], FA [13] and particle swarm optimization (PSO). All these techniques have the same iterations number $k_{\max} = 1000$ and population size $i = 100$. The average results of these optimization techniques for 20 runs are reported in Table 3, which shows the RE of each variable and fitness value $C(\hat{p})$. The results in Table 3 have also verified that the CFOA outperforms the other optimization techniques as CFOA has the lowest fitness $C(\hat{p})$. Average RE of each variable using these techniques shown in Table 3 also confirm the best performance of proposed CFOA technique among these optimization techniques.

Now, the identified system model will be established using the optimal identified values p^* by CFOA technique in Table 1. Figs. 8 and 9 show the measured outputs (y_1 and y_2) and the corresponding model outputs using p^*. The output errors between the measured outputs and the corresponding model outputs are also shown. It can be seen from Figs. 8 and 9 that the model outputs using p^* reflects the actual outputs well. This indicates that the CFOA based identification technique has reached good results compared with the actual system outputs.

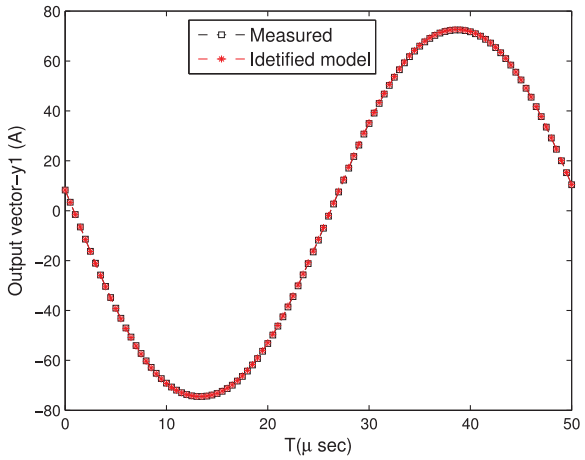

(a) Measured and identified model output of y_1

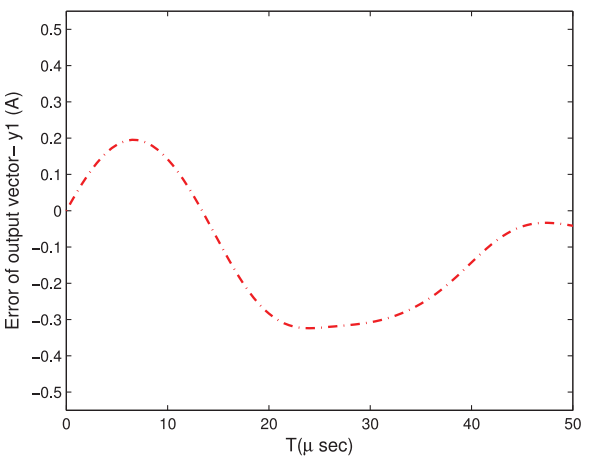

(b) Error of output vector y_1

Fig. 8. Measured and identified result of y_1.

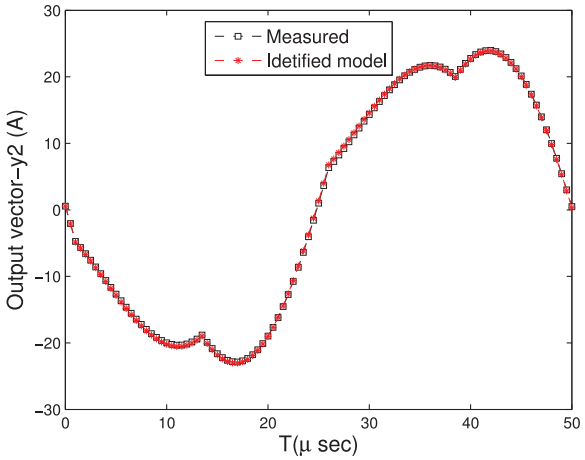

(a) Measured and identified model output of y_2

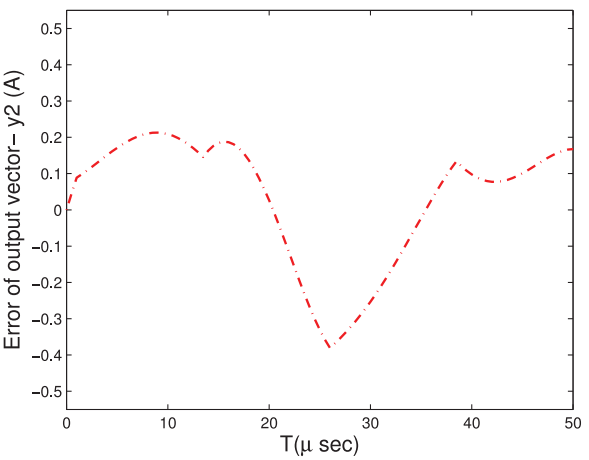

(b) Error of output vector y_2

Fig. 9. Measured and identified result of y_2.

In addition to the output vectors, the state vectors have also been tested. Fig. 10 has illustrated the actual state vector and the model state vector using the optimal identified values p^* for this sample data. The comparison performance for these state vectors also shows that the difference between the actual and identified model values is very small.

6.2. Case 2: Performance analysis of parameter identification with measurement noise

To examine the robustness of the proposed identification technique, measurement noise are considered in this case. 5% random noise is applied to the output vectors y_1 and y_2, as illustrated in Fig. 11. Then output vectors y_1 and y_2 with 5% random noise are used in the parameter identification problem as in Eq. (36). Other system parameters and CFOA parameters take the same value as in Case 1.

The optimal identified values p^* with 5% random measurement noise by CFOA technique using Tent chaotic sequence are summarized in Table 4. In Table 4, comparison among actual p and optimal identified values p^* of this system has been reported. Meanwhile, IAE and RE for each variable have also been reported. It can be seen from Table 4 that the unknown parameters are correctly identified by the proposed CFOA technique, and the difference between the actual values and the identified ones is very small even when the measurement noise exists.

Now, the simulation results of CFOA technique using different chaotic sequences are also tested with measurement noise. The average results of the CFOA technique using different chaotic sequences for 20 runs are reported in Table 5, which shows the RE of each variable and fitness value $C(\hat{p})$. The results in Table 5 have also verified that CFOA technique using different chaotic sequences can reach a good result, the difference between different chaotic sequences is very little.

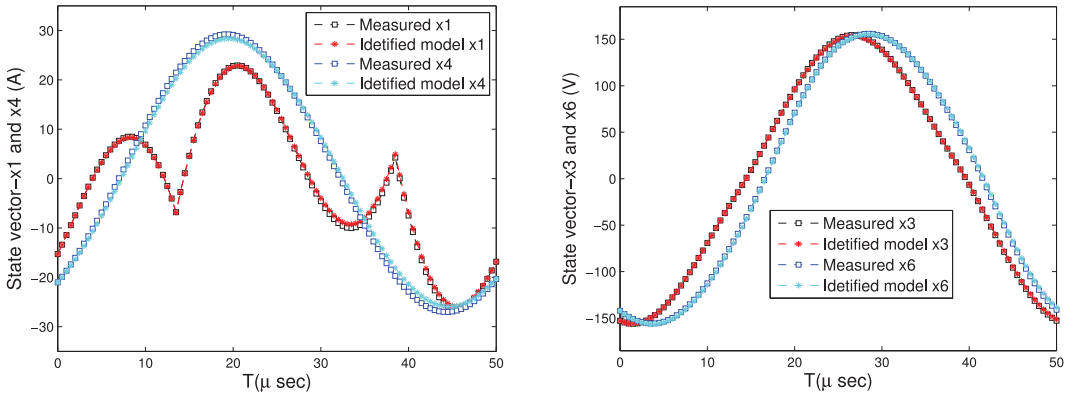

(a) Measured and identified model value of x_1 and x_4 (b) Measured and identified model value of x_3 and x_6

Fig. 10. Measured and identified result of state vectors.

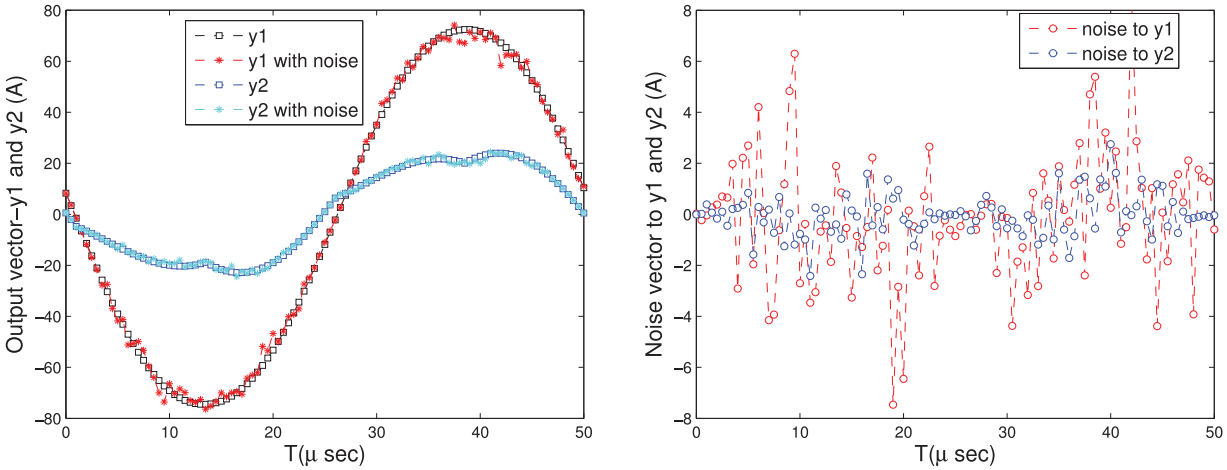

(a) y_1 and y_2 with or without noise (b) Noise added to y_1 and y_2

Fig. 11. 5% random measurement noise added to y_1 and y_2 for sample dataset.

Table 4
Comparison among actual p and optimal identified values p^* with measurement noise by CFOA technique.

Item	L_{pi}	L_T	L_{si}	L_{so}	C_T	C_s	M	R_{pi}	R_T	R_{si}	R_{so}
Unit	μH	μH	μH	μH	μF	μF	μH	Ω	Ω	Ω	Ω
Actual p	14.01	13.7	27.3	27.1	4.7	2.43	8.0	0.0152	0.0158	0.0179	0.0122
Identified p^*	13.81	13.64	27.59	26.44	4.72	2.41	8.19	0.0162	0.0145	0.0192	0.0131
IAE	0.20	0.06	0.29	0.66	0.02	0.02	0.19	0.0010	0.0013	0.0013	0.0009
RE (%)	1.43	0.44	1.06	2.44	0.43	0.82	2.38	6.57	8.23	7.26	7.37

Table 5
Parameter identification simulation results using different chaotic sequences for CFOA technique.

Chaotic	RE (%)											Fitness
sequence	L_{pi}	L_T	L_{si}	L_{so}	C_T	C_s	M	R_{pi}	R_T	R_{si}	R_{so}	$C(\hat{p})$
Logistic	1.78	2.27	1.92	2.49	2.76	2.17	2.09	5.72	5.90	5.86	6.14	**17.35**
Tent	1.57	1.73	1.88	2.23	2.41	2.30	2.15	5.63	5.47	5.21	5.52	**17.13**
Chebyshev	2.13	1.94	2.25	2.07	2.81	2.05	2.59	5.58	5.83	5.49	6.03	**17.29**
Cubic	1.86	2.02	2.07	1.78	2.55	1.92	2.07	5.18	6.33	5.40	5.36	**17.65**
ICMIC	1.75	1.92	2.18	2.14	2.25	2.09	2.15	5.60	5.80	5.72	6.09	**17.12**
Sinusodial	1.96	2.17	2.11	1.90	2.49	2.35	1.94	5.76	6.02	6.08	5.86	**17.36**

Table 6
Parameter identification simulation results using different optimization techniques.

Optimization technique	RE (%)											Fitness
	L_{pi}	L_T	L_{si}	L_{so}	C_T	C_s	M	R_{pi}	R_T	R_{si}	R_{so}	$C(\hat{p})$
FOA	3.54	3.60	3.38	4.11	4.07	4.36	3.47	9.15	10.21	8.44	8.30	**38.27**
CFOA	1.57	1.73	1.88	2.23	2.41	2.30	2.15	5.63	5.47	5.21	5.52	**17.13**
ACO	2.52	3.35	2.96	3.35	3.53	3.49	3.08	6.61	7.18	7.29	7.45	**27.48**
ABC	2.79	2.93	3.14	3.07	3.42	3.28	3.29	6.39	7.16	6.80	7.32	**26.03**
GA	2.44	2.56	2.58	3.22	2.94	3.07	2.77	6.31	6.08	6.20	6.39	**22.94**
FA	2.68	3.01	2.87	3.19	3.50	3.31	3.48	6.24	6.53	6.52	7.27	**26.59**
PSO	2.03	2.26	2.19	2.67	2.33	2.73	2.25	5.50	5.59	5.72	6.11	**19.22**

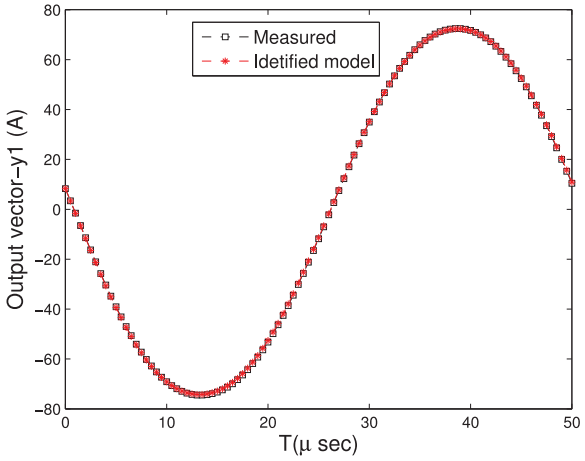

(a) Measured and identified model output of y_1

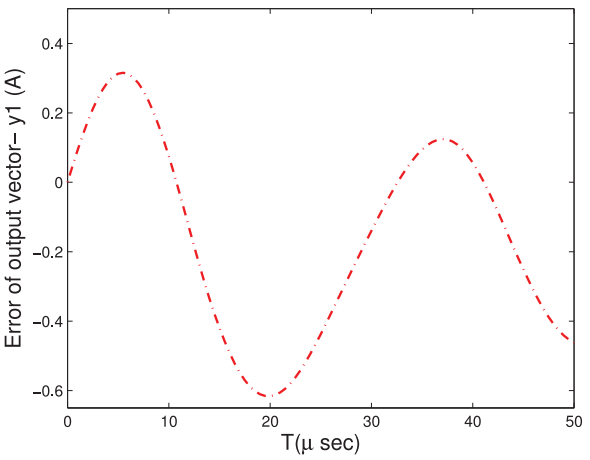

(b) Error of output vector y_1

Fig. 12. Measured and identified result of y_1.

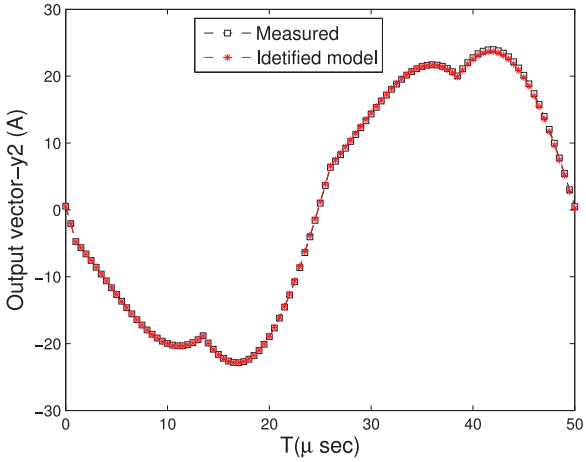

(a) Measured and identified model output of y_2

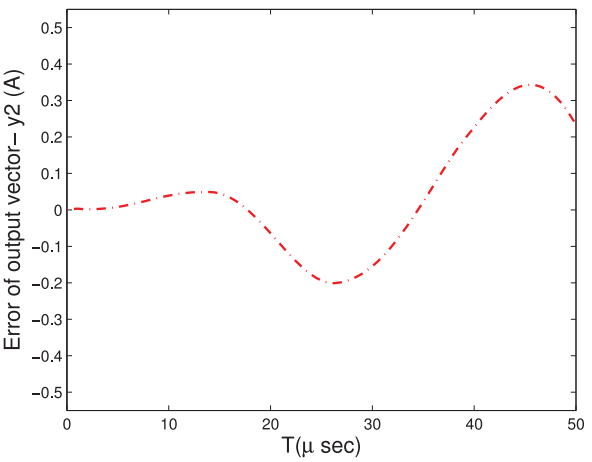

(b) Error of output vector y_2

Fig. 13. Measured and identified result of y_2.

Here the simulation results with measurement noise using different optimization techniques are also compared. The average results of these optimization techniques for 20 runs are reported in Table 6, which also shows that the CFOA technique outperforms other optimization techniques as CFOA has the lowest fitness $C(\hat{p})$. Average RE of each variable using these optimization techniques shown in Table 6 also confirms the good performance of proposed CFOA technique.

Now, the identified model of this system is established using the optimal identified values p^* by CFOA technique in Table 4. Figs. 12 and 13 show the measured outputs and the corresponding model outputs using the optimal identified values p^*. The output errors between the measured and the corresponding model outputs are also shown. Although the identified system model

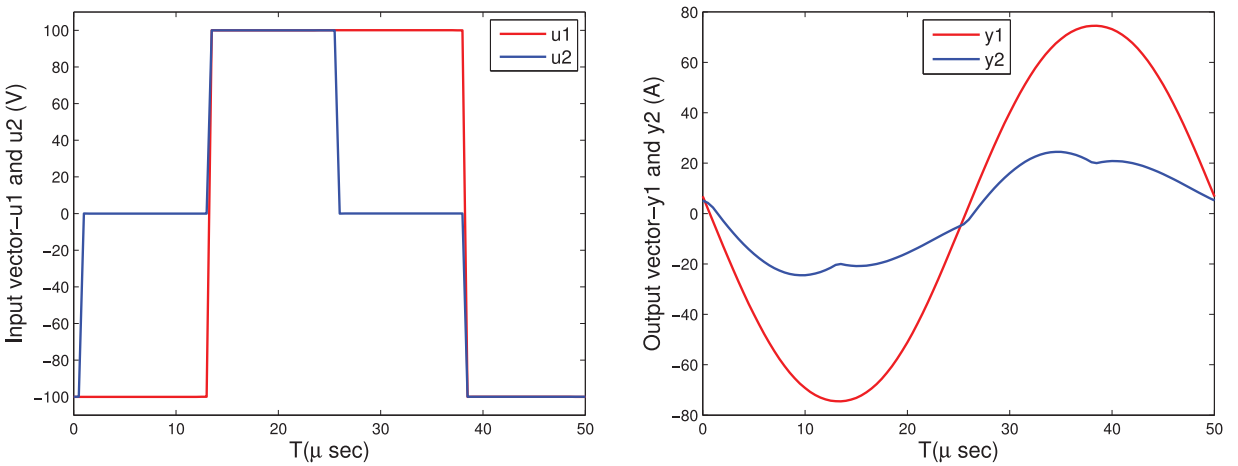

(a) Varied input vector u_1 and u_2 (b) Measured output vector y_1 and y_2

Fig. 14. Varied input and output vectors for generalization ability test.

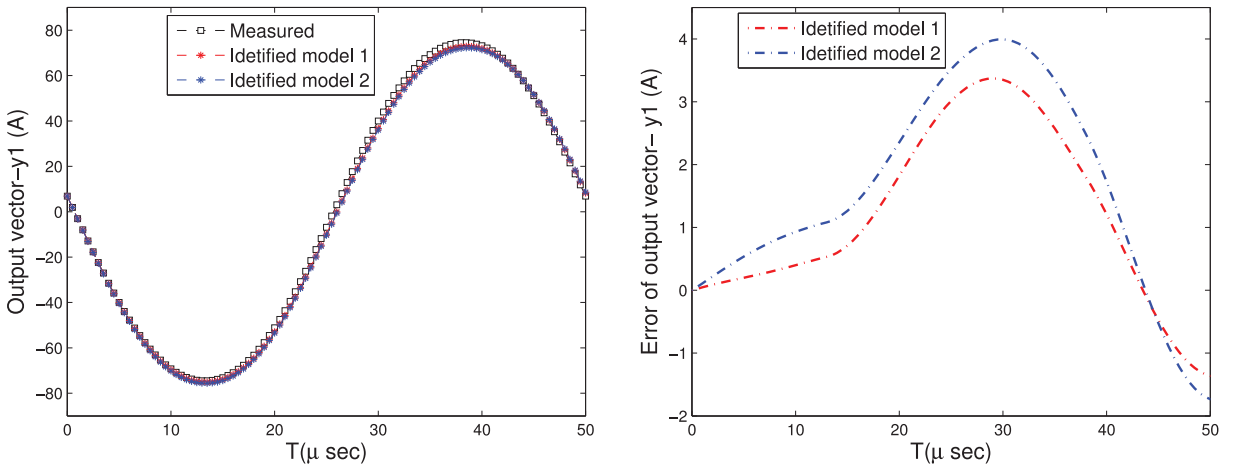

(a) Measured and identified model output of y_1 (b) Error of output vector y_1

Fig. 15. Measured and identified result of y_1.

is derived from the sample dataset with measurement noise, the model outputs using p^* reflects the actual outputs well. This indicates that the CFOA based identification technique has good robustness against the measurement noise.

6.3. Case 3: Performance in varied operation condition

To examine the generalization ability of the proposed CFOA technique, the identified results of this system are tested in varied operation condition. Here, varied input vectors u_1 and u_2 with the number of 100 samples are applied, which are illustrated in Fig. 14(a). In this operation condition, the output vector y_1 and y_2 of BIPT system are measured as in Fig. 14(b). It can seen from Fig. 14 that the input and output vectors are different from that in Cases 1 and 2. We will test whether the optimal identified values p^* in Cases 1 and 2 are valid in this condition.

In this operation condition, the system model outputs using p^* in Cases 1 and 2 are compared with the measured outputs, which are illustrated in Figs. 15 and 16. Here two identified models are compared, the 'identified model 1' denotes the system model constructed based on p^* by CFOA technique in Case 1, and the 'identified model 2' denotes the system model constructed based on p^* with measurement noise by CFOA technique in Case 2. It can be seen from Figs. 15 and 16 that the two identified models' outputs are close to the actual outputs. This also means that the identified models have good generalization ability in other operation condition.

Here, output errors of y_1 and y_2 of the optimal identified values using different optimization techniques are also compared, and the root-mean-square error (RMSE) is used to quantify the error. The compared simulation results of the optimal identified values using different optimization techniques have been reported in Table 7. From Table 7, it is straight-forward to see that the

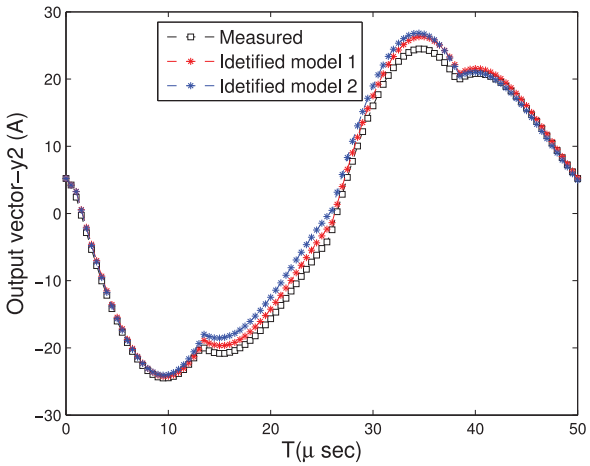

(a) Measured and identified model output of y_2

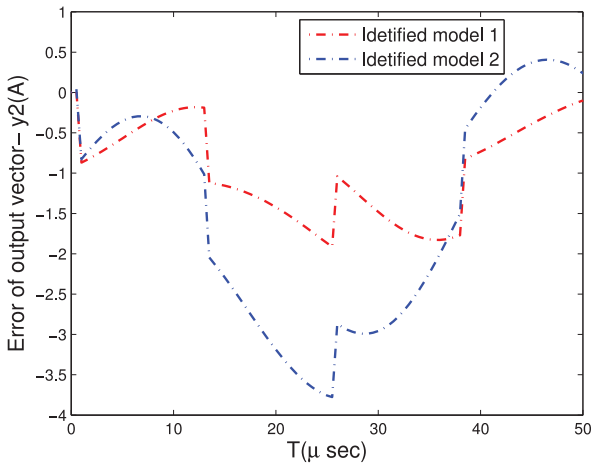

(b) Error of output vector y_2

Fig. 16. Measured and identified result of y_2.

Table 7
Compared output errors of y_1 and y_2 using different optimization techniques.

	Identified model 1							Identified model 2						
Item	FOA	CFOA	ACO	ABC	GA	FA	PSO	FOA	CFOA	ACO	ABC	GA	FA	PSO
RMSE of y_1	0.45	0.21	0.31	0.27	0.23	0.30	0.22	0.47	0.22	0.33	0.28	0.25	0.31	0.23
RMSE of y_2	0.38	0.17	0.25	0.22	0.19	0.25	0.19	0.39	0.18	0.27	0.23	0.21	0.27	0.19

CFOA technique has the lowest RMSE value for both y_1 and y_2 among these seven optimization techniques. This also means that the proposed CFOA technique has the best generalization ability for this problem. In Table 7, the RMSEs of CFOA are much less than RMSEs of FOA, this has verified the good performance of the proposed CFOA.

From the simulation results in Cases 1–3, it follows that the CFOA based identification technique has the best identification results among these seven optimization techniques (FOA, CFOA, ACO, ABC, GA, FA, PSO). As the CFOA is the improvement to original FOA, we also find that CFOA has improved the exploration and exploitation ability of FOA. For the CFOA, six kinds of different chaotic sequences are compared and the results show that different chaotic sequences can be applied in the proposed CFOA technique.

7. Conclusions

The main contribution of this paper is establishing a novel CFOA technique, and it is applied to parameter identification in BIPT system. The simulation results shows that the unknown parameter values are correctly identified and the difference between the estimated values and measured ones is very small. Compared with other optimization techniques, the proposed CFOA has less identification error. Six kinds of different chaotic sequences are compared, and there is little difference between different chaotic sequences. The simulation results also show that the proposed CFOA technique is robust to measurements noise and variation of operation condition and thus it is suitable for practical application.

References

[1] C.S. Wang, O.H. Steilau, G.A. Covic, Design considerations for a contactless electric vehicle battery charger, IEEE Trans. Ind. Electr. 52 (5) (2005) 1308–1314.
[2] U.K. Madawala, D.J. Thrimawithana, N. Kularatna, An ICPT-supercapacitor based hybrid system for surge free power transfer, IEEE Trans. Ind. Electr. 54 (6) (2007) 3287–3297.
[3] A.K. Swain, M.J. Neath, U.K. Madawala, D.J. Thrimawithana, A dynamic model for bi-directional inductive power transfer systems, in: Proceedings: IECON 2011, vol. 1, 2011, pp. 1024–1029.
[4] U.K. Madawala, D.J. Thrimawithana, A bidirectional inductive power interface for electric vehicles in V2G systems, IEEE Trans. Ind. Electr. 58 (10) (2011) 4789–4796.
[5] A.K. Swain, M.J. Neath, U.K. Madawala, D.J. Thrimawithana, A dynamic multivariable state-space model for bidirectional inductive power transfer systems, IEEE Trans. Power Electr. 27 (1) (2012) 4772–4780.
[6] H. Zang, S. Zhang, K. Hapeshi, A review of nature-inspired algorithms, J. Bionic Eng. 7 (S) (2010) S232–S237.
[7] B.C. Mohan, R. Baskaran, A survey: Ant colony optimization based recent research and implementation on several engineering domain, Exp. Syst. Appl. 39 (4) (2012) 4618–4627.
[8] C. Changdar, G.S. Mahapatra, R.K. Pal, An ant colony optimization approach for binary knapsack problem under fuzziness, Appl. Math. Comput. 233 (2013) 243–253.
[9] M.S. Kiran, O. Findik, A directed artificial bee colony algorithm, Appl. Soft Comput. 26 (2015) 454–462.

[10] K. Ayan, U. Kilic, Artificial bee colony algorithm solution for optimal reactive power flow, Appl. Soft Comput. 12 (5) (2012) 1477–1482.
[11] V. Ahuja, R.J. Hartfield, A. Shelton, Optimization of hypersonic aircraft using genetic algorithms, Appl. Math. Comput. 242 (2014) 423–434.
[12] M. Thakur, S.S. Meghwani, H. Jalota, A modified real coded genetic algorithm for constrained optimization, Appl. Math. Comput. 235 (2014) 292–317.
[13] A.H. Gandomi, X.S. Yang, A.H. Alavi, Mixed variable structural optimization using firefly algorithm, Comput. Struct. 89 (23-24) (2011) 2325–2336.
[14] T.J. Hsieh, A bacterial gene recombination algorithm for solving constrained optimization problems, Appl. Math. Comput. 231 (2014) 187–204.
[15] Y. Marinakis, M. Marinaki, Combinatorial neighborhood topology bumble bees mating optimization for the vehicle routing problem with stochastic demands, Soft Comput. 19 (2) (2015) 353–373.
[16] J.J.Q. Yu, V.O.K. Li, A social spider algorithm for global optimization, Appl. Soft Comput. 30 (2015) 614–627.
[17] W.T. Pan, A new fruit fly optimization algorithm: taking the financial distress model as an example, Knowl.-Based Syst. 26 (1) (2012) 69–74.
[18] F. Bartumeus, M.G.E.d. Luz, G.M. Viswanathan, J. Catalan, Animal search strategies: A quantitative random walk analysis, Ecology 86 (11) (2005) 3078–3087.
[19] A.M. Reynolds, M.A. Frye, Free-flight odor tracking in *Drosophila* is consistent with an optimal intermittent scale-free search, PLoS ONE 2 (4) (2007) e354.
[20] S.M. Lin, Analysis of service satisfaction in web auction logistics service using a combination of fruit fly optimization algorithm and general regression neural network, Neural Comput. Appl. 22 (3-4) (2013) 783–791.
[21] W. Sheng, Y. Bao, Fruit fly optimization algorithm based fractional order fuzzy-PID controller for electronic throttle, Nonlinear Dynam. 73 (1-2) (2013) 611–619.
[22] J.Q. Li, Q.K. Pan, K. Mao, P.N. Suganthan, Solving the steelmaking casting problem using an effective fruit fly optimisation algorithm, Knowl.-Based Syst. 72 (2014) 28–36.
[23] J.Y. Zhao, X.F. Yuan, Multi-objective optimization of stand-alone hybrid PV-wind-diesel-battery system using improved fruit fly optimization algorithm, Soft Comput. (2015), doi:10.1007/s00500-015-1685-6.
[24] Y. Xing, Design and optimization of key control characteristics based on improved fruit fly optimization algorithm, Kybernetes 42 (3) (2013) 466–481.
[25] W.T. Pan, Using modified fruit fly optimisation algorithm to perform the function test and case studies, Connect. Sci. 25 (2-3) (2013) 151–160.
[26] L. Wang, X.L. Zheng, S.Y. Wang, A novel binary fruit fly optimization algorithm for solving the multidimensional knapsack problem, Knowl.-Based Syst. 48 (2013) 17–23.
[27] X. Yuan, X. Dai, J. Zhao, Q. He, On a novel multi-swarm fruit fly optimization algorithm and its application, Appl. Math. Comput. 233 (2014) 260–271.
[28] D.X. Yang, G. Li, G. D.Cheng, On the efficiency of chaos optimization algorithms for global optimization, Chaos Soliton Fractal 34 (4) (2007) 1366–1375.
[29] D.X. Yang, Z.J. Liu, J.L. Zhou, Chaos optimization algorithms based on chaotic maps with different probability distribution and search speed for global optimization, Commun. Nonlinear Sci. Numer. Simul. 19 (4) (2014) 1229–1246.
[30] M. Wan, C. Wang, L.X. Li, Y.X. Yang, Chaotic ant swarm approach for data clustering, Appl. Soft Comput. 12 (8) (2012) 2387–2393.
[31] X. Yuan, J. Zhao, Y. Yang, Y. Wang, Hybrid parallel chaos optimization algorithm with harmony search algorithm, Appl. Soft Comput. 17 (2014) 12–22.
[32] X. Yuan, S. Li, Y. Wang, W. Sun, L. Wu, Parameter identification of electronic throttle using a hybrid optimization algorithm, Nonlinear Dynam. 63 (4) (2011) 549–557.